⌘ *Author's Choice*

THE JOURNAL OF BIOLOGICAL CHEMISTRY VOL. 286, NO. 27, pp. 23852–23864, July 8, 2011

The Linker Region of MacroH2A Promotes Self-association of Nucleosomal Arrays*[S]

Received for publication, March 28, 2011, and in revised form, April 27, 2011 Published, JBC Papers in Press, April 30, 2011, DOI 10.1074/jbc.M111.244871

Uma M. Muthurajan[‡], Steven J. McBryant[§], Xu Lu[¶], Jeffrey C. Hansen[‡], and Karolin Luger[‡‖1]

From the [‡]Department of Biochemistry and Molecular Biology and the [‖]Howard Hughes Medical Institute, Colorado State University, Fort Collins, Colorado 80523, [§]Gevo Inc., Englewood, Colorado 80112, and the [¶]University of Findlay, Findlay, Ohio 45840

MacroH2A is a histone variant found in higher eukaryotes localized at the inactive X chromosome and is known to maintain heterochromatic regions in the genome. MacroH2A consists of a conserved histone domain and a macro domain connected by a linker region. To understand the contributions of the three domains to chromatin condensation, we incorporated various constructs of macroH2A into defined nucleosomal arrays and analyzed their impact on *in vitro* chromatin compaction. The folding and oligomerization properties of arrays containing full-length macroH2A (macroH2A$_{FL}$), macroH2A(1–161) (encompassing the histone domain and linker region), and macroH2A(1–122) (histone domain only) were compared with major-type H2A arrays. Analytical ultracentrifugation and atomic force microscope imaging indicate that macroH2A(1–161)-containing arrays favor condensation under conditions where major-type arrays are nearly fully extended. In contrast, arrays with macroH2A$_{FL}$ exhibit behavior similar to that of major-type arrays. This suggests that the linker region of macroH2A facilitates array condensation and that this behavior is inhibited by the macro domain. Furthermore, chimeric major-type H2A arrays containing the macroH2A linker domain (H2A$_{ML}$) exhibited the same condensation properties as macroH2A(1–161) arrays, thus emphasizing the intriguing behavior of the macroH2A linker region.

Chromatin architecture is altered locally or globally through the incorporation of histone variants, distinct non-allelic variants that replace major-type histones in nucleosomes at certain locations in the genome. Histone variants exist in all eukaryotic tissues. The largest number of histone variants has been described for histone H2A (1, 2). Among these, macroH2A is arguably the most unusual because it is about 3 times the size of major-type H2A, through the addition of a non-histone "macro domain" that is connected to the histone domain by a flexible linker region (3) (Fig. 1*A*). MacroH2A is preferentially localized on the inactive X chromosome in female mammals, where it contributes to the maintenance of a transcriptionally repressed state. However, recent work has shown that, depending on context, macroH2A can either activate or repress transcription of genes that are not located on the X chromosome (4). MacroH2A has also been observed in other facultative heterochromatic regions like the pericentromere, the XY body of spermatocytes, and senescence-related heterochromatin (5, 6). The repressive behavior of macroH2A was recently implicated in suppressing melanoma progression through regulation of CDK8 (7). It is currently unknown which structural property of macroH2A conveys the propensity to form repressive chromatin structures.

MacroH2A has a unique tripartite structure. The N-terminal histone domain (residues 1–122) is connected to a C-terminal macro domain (residues 162–371) via a flexible ~40-amino acid linker region (residues 123–161) (Fig. 1*A*). The histone fold domain is 64% identical to major-type H2A and contains elements that direct macroH2A to the inactive X chromosome (8). X-ray crystallographic studies have revealed that the main differences between major-type H2A and macroH2A-containing nucleosomes are in the L1 loop region that forms the only H2A-H2A contact within the nucleosome (3). Subsequent studies have shown that macroH2A preferentially forms heterotypic nucleosomes containing one canonical H2A-H2B dimer and one macroH2A-H2B dimer together with an $(H3\text{-}H4)_2$ tetramer (9). The composition of macroH2A-containing nucleosomes *in vivo* has not yet been resolved, and a macroH2A-specific histone chaperone is yet to be identified.

The macro domain is found in several proteins in bacteria, viruses, archea, and eukaryotes, where it is implicated in many diverse functions. The macro domain in macroH2A is ~25 kDa and is roughly spherical, consisting of seven parallel and antiparallel β-sheets connected via six α-helices (Protein Data Bank code 1YD9) (3). In vertebrates, this domain is often fused to other proteins and is involved in ADP-ribosylation or poly-(ADP-ribose) polymerization (10). MacroH2A exists in two different forms, macroH2A1 and -2. MacroH2A1 further has two splice variants, macroH2A1.1 and -1.2. The three forms (macroH2A1.1, macroH2A1.2, and macroH2A2) vary in the amino acid sequence in the macro domain and ADP-ribose binding abilities of the macro domain, whereas the histone fold domain and the linker region are identical among the three protein isoforms (11). In the studies conducted in the present report, human macroH2A1.2 was used.

The 40-amino acid linker region connecting the histone fold domain with the macro domain exhibits many features of an intrinsically disordered protein (12). It has an amino acid composition typically found in disordered regions, characterized by a conspicuous absence of certain hydrophobic amino acids.

* This work was supported, in whole or in part, by National Institutes of Health Grants GM061909 and P01GM088409 (to K. L.) and GM45916 (to J. C. H.).

[S] The on-line version of this article (available at http://www.jbc.org) contains supplemental Figs. 1–4 and supplemental references.

⌘ *Author's Choice*—Final version full access.

[1] Supported by the Howard Hughes Medical Institute. To whom correspondence should be addressed. Tel.: 970-491-6405; Fax: 970-491-5113; E-mail: karolin.luger@colostate.edu.

TABLE 1

Amino acid composition of mouse major-type H2A (PubMed accession number P22752) C terminus, mouse H1° C terminus (12), and the linker region of human macroH2A1.2 (3)

The linker histone C terminus and macroH2A linker region have fewer order-producing amino acids and a higher proportion of disorder-causing amino acids, leading to their classification as intrinsically disordered proteins (12).

	H2A C-terminal domain (92–130)	H1° C-terminal domain (residues 97–193)[a]	MacroH2A linker region (residues 123–160)[b]
No. of amino acids	38	97	38
Percentage disorder-producing (K/P/G/R/N/Q/S/E/D/M)	52.6	73.6	74
Percentage order-producing (V/H/F/I/L/C/W/Y)	34.2	1	10

[a] Ref. 12.
[b] Ref. 3.

Only 10% (4 of 38 amino acids) of the amino acid residues present within the linker region can be classified as "order-inducing" (*e.g.* Val, His, Phe, Tyr, etc.). Thus, the linker domain closely resembles the intrinsically disordered C-terminal tail of linker histone H1 (Table 1 and supplemental material) (12). In contrast, 35% of all residues in the much shorter C-terminal tail of major-type H2A are order-inducing residues (Table 1). Previous studies have shown that the C-terminal tail of H1 is essential for the chromatin-condensing properties of linker histones and that the specific amino acid composition rather than the precise sequence of this region is required for molecular recognition and function (13). Whether the compositional similarities between the macroH2A linker region and the H1 C-terminal region translate into functional similarities has not yet been explored.

Here we investigate the contributions of the histone domain, the linker region, and the macro domain of macroH2A in the formation of condensed chromatin structures *in vitro*. We apply analytical ultracentrifugation (AUC)[2] and atomic force microscopy (AFM) to study the *in vitro* folding and self-assembly properties of defined nucleosomal arrays. We show that nucleosomal arrays reconstituted with macroH2A$_{FL}$ exhibit condensation properties that are similar to those reconstituted with major-type H2A but that deletion of the macro domain promotes dramatic oligomerization of nucleosome arrays. A chimeric histone generated by attaching the macroH2A linker region to the C terminus of major-type H2A shows that this property is exclusively a function of the macroH2A linker region.

EXPERIMENTAL PROCEDURES

Protein Expression and Purification—MacroH2A$_{FL}$ (human macroH2A1.2) was co-expressed in bacteria with H2B (mouse) in a CDFDuet-1 vector. This adds a C-terminal hexahistidine tag on macroH2A. The plasmid was transformed into *Escherichia coli* BL21 (DE3) cells, grown to an A_{600} of 0.4 at 37 °C, and induced overnight at 25 °C using the Dual Media Expression system (Zymo Research). MacroH2A$_{FL}$-H2B dimer was batch-purified over nickel resin followed by gel filtration over a Superdex 200 column in the presence of 2 M NaCl.

All other histones (H2A, H2B, H3, H4, macroH2A(1–122), macroH2A(1–161), and H2A with macro linker (H2A$_{ML}$)) were of mouse origin and were expressed from either pET3a or pET5a vectors and purified from inclusion bodies as described (14). The expression vector for H2A$_{ML}$ was obtained from GeneArt. All histones (with the exception of macroH2A$_{FL}$-H2B dimers) were refolded as described (14).

Nucleosomal Array Assembly—Nucleosomal arrays were assembled on a DNA fragment containing 12 repeats of the 207-base pair "601" positioning sequence (15). Assemblies were performed with H2A-H2B (or macroH2A-H2B) dimers, (H3-H4)$_2$ tetramer, and DNA in a two-step reconstitution. Previous studies have shown that macroH2A(1–122) octamer does not dissociate into dimers and tetramers at the appropriate ionic strength during salt gradient deposition, resulting in non-canonical nucleosomes (9). In the first step, varying amounts of (H3-H4)$_2$ tetramer were added to DNA, followed by step dialysis (4–6 h for each step) starting from 1 M NaCl, 0.75 M NaCl, and finally 2.5 mM NaCl (in 10 mM Tris, pH 7.5, 0.25 mM EDTA), to obtain tetrasome arrays. The optimal ratio of DNA to (H3-H4)$_2$ tetramer was determined by performing sedimentation velocity AUC (described in detail below) of the individual experiments, with a target midpoint $s_{20,w}$ of ~19 (supplemental Fig. 4*A*) (16) and EcoRI digestion (not shown). In the second step, nucleosomes were assembled by adding increasing amounts of H2A-H2B (or macroH2A-H2B) dimer to the optimized (H3-H4)$_2$ tetramer/DNA ratio and dialyzed as described above. The saturation level of the arrays was analyzed by sedimentation velocity and confirmed using EcoRI digestion (17) (supplemental Fig. 1, *A* and *B*, respectively).

Undersaturated arrays were assembled in a similar fashion with the difference that in the first step fewer tetrasomes were incorporated to yield 13–14 S arrays, and then macroH2A(1–161) dimers were titrated with increasing *R* values (0.8–1.4). The *R* value is defined as the proportion of macroH2A(1–161)-H2B dimer added per 207-bp nucleosomal DNA repeat. For obtaining 25–29 S arrays, a typical R value of dimers was 2–2.5.

Sedimentation Velocity—To determine the nucleosome density on arrays and to monitor $MgCl_2$-dependent array folding, nucleosomal arrays were subjected to sedimentation velocity AUC in either the An50Ti or An60Ti rotor using a Beckman XL-A or XL-I ultracentrifuge at 18–22,000 rpm and 21 °C. The arrays were detected with the absorbance optical system at 259 nm in the continuous scanning mode with a radial increment of 0.003 cm. The resulting boundaries were analyzed using the improved van Holde-Weischet method as implemented in Ultrascan version 8.0 (18). This analysis results in a diffusion-corrected integral distribution ($G(s)$) of sedimentation coefficients over the entire boundary ($s_{20,w}$ is the sedimentation coefficient corrected for temperature and normalized to water). This is shown to be precise in examining the solution behavior

[2] The abbreviations used are: AUC, analytical ultracentrifugation; AFM, atomic force microscopy.

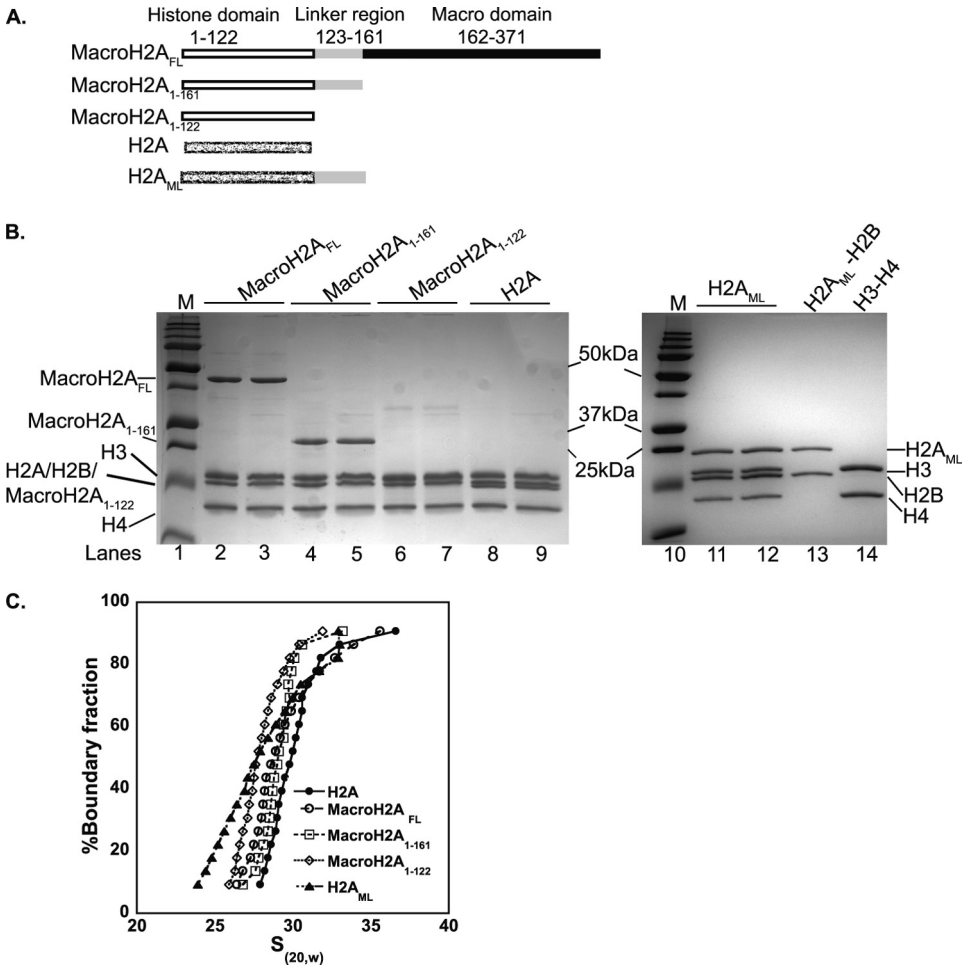

FIGURE 1. **MacroH2A constructs and array assembly.** *A*, macroH2A constructs used in the present study: macroH2A$_{FL}$ (residues 1–371), macroH2A(1–161) (histone + linker domains), macroH2A(1–122) (histone domain), H2A (major-type H2A of mouse origin 1–130), and H2A$_{ML}$ (major-type H2A with the linker region of macroH2A attached to its C terminus). *B*, arrays assembled with the various constructs shown in *A* were analyzed by 15% SDS-PAGE to verify the equimolar distribution of histones. *Lanes 1* and *10*, protein size markers (*M*); *lanes 13* and *14*, H2A$_{ML}$-H2B dimer and H3-H4 tetramer, respectively. *C*, sedimentation velocity *G*(*s*) curves for saturated arrays with 50% $s_{20,w}$ ~27–29 S in a 10 mM Tris, pH 7.5, 0.25 mM EDTA, 2.5 mM NaCl buffer. All arrays have a small percentage of oversaturated population that is >30 S.

of model nucleosome arrays (19). For folding experiments, $MgCl_2$ was added to the arrays to final concentrations of 0.5, 0.75, and 1.0 mM prior to AUC by adding equal volumes of 2× $MgCl_2$ stocks.

To demonstrate the reversibility of the oligomerization of macroH2A(1–161) arrays, they were treated with 1.0 mM $MgCl_2$ and then dialyzed in 10 mM Tris (pH 7.5), 0.25 mM EDTA, and 2.5 mM NaCl buffer overnight to remove the magnesium chloride, prior to subjecting them to a sedimentation velocity experiment, as described above.

Nucleosomal Array Self-association—Self-association assays were performed as described previously (20, 21).

AFM Imaging and Image Analysis—AFM imaging of nucleosomal arrays was performed in air using an Asylum Research MFP-3D Atomic Force Microscope, on an 3-aminopropyltriethoxysilane modified mica surface. 2 × 2 μm scans were collected with 512 scan lines. Olympus 240TS tips were routinely used for imaging. Samples were diluted appropriately (to ~1.5 ng/μl) and a ~30-μl drop was allowed to sit on the 3-aminopropyltriethoxysilane surface for ~15 min at room temperature. After 15 min, the sample was rinsed off with the indicated buffer (10 mM Tris, pH 7.5, 0.25 mM EDTA, 2.5 mM NaCl; with 0.5 mM $MgCl_2$ for magnesium chloride-treated samples for visualizing folding experiments). Images were flattened and analyzed using the MFP-3D software provided by Asylum. Each image was divided into four quadrants and zoomed in digitally to obtain a clearer view of well separated arrays, and multiple free hand lines were drawn through the arrays, and height profiles were obtained for the nucleosomes (*e.g.* supplemental Fig. 3*C*). Several such images were analyzed for each type of array encompassing several hundreds of nucleosomes. Height profiles were recorded, categorized, and plotted in MS Excel.

RESULTS

The Macro Domain and Linker Region of MacroH2A Do Not Affect the Assembly of Nucleosomal Arrays in Vitro—To assess the contributions of the three macroH2A domains (Fig. 1A) on the structural transitions of defined nucleosomal arrays, we prepared two truncated versions of macroH2A. MacroH2A(1–161) lacks only the macro domain, leaving the linker region (amino acids 123–161) intact, whereas in macroH2A(1–122), both the macro domain and the linker region were deleted,

leaving only the histone domain. To isolate the contributions of the linker region, we also prepared a version of H2A in which the macroH2A linker region (residues 123–161) was added to the C terminus of major-type H2A ($H2A_{ML}$; Fig. 1*A*).

$MacroH2A_{FL}$ was co-expressed with H2B, and the macroH2A-H2B dimer was purified from the soluble fraction of bacterial lysates. All nucleosomal arrays were prepared from individually refolded H2A-H2B (or variant H2A-H2B) dimers and $(H3\text{-}H4)_2$ tetramers using a two-step reconstitution method. Briefly, purified $(H3\text{-}H4)_2$ tetramers were titrated onto the 601 207-12 DNA to give rise to tetrasome arrays with a midpoint $s_{20,w}$ of ~19 (supplemental Fig. 4*A*), the expected sedimentation coefficient for 12 tetramers bound to each available positioning site (22). The 19 S tetrasome arrays were further assembled with 2 molar equivalents of dimers composed of H2B with either H2A, macroH2A, or one of the truncated macroH2A versions. To test whether the assembled arrays contained all four histones in stoichiometric amounts, the protein content of the arrays was analyzed by SDS-PAGE (Fig. 1*B*). The equimolar stoichiometry of the four histones was evident in full-length (*lanes 2* and *3*) and macroH2A(1–161) arrays (*lanes 4* and *5*) as well as in $H2A_{ML}$ arrays (*lanes 11* and *12*). MacroH2A(1–122) co-migrates with H3 (~16 kDa; *lanes 6* and *7*). Similarly reconstituted major-type H2A-containing arrays were loaded as a control (*lanes 8* and *9*). This analysis clearly demonstrated that each assembled array contains the full complement of core histones in the correct stoichiometry.

The number of nucleosomes on the DNA template (defined as the saturation level of the arrays, 12 nucleosomes for a fully saturated array) affects nucleosome array oligomerization and folding (20). Therefore, all arrays were carefully matched for their level of saturation, as judged by both sedimentation velocity in low salt and by EcoRI digestion (Fig. 1*C* and supplemental Fig. 1, *A* and *B*). The midpoint $s_{20,w}$, defined as the *s* value at 50% boundary fraction, as derived from experiments such as shown in Fig. 1*C*, is a convenient measure for comparing the saturation levels of various arrays. We prepared subsaturated arrays (with an average of 10 ± 2 nucleosomes and a midpoint $s_{20,w}$ of ~25) (supplemental Fig. 1*A*) as well as saturated arrays (with an average of 11.5 ± 2 nucleosomes and a midpoint $s_{20,w}$ of ~28) with all H2A and macroH2A constructs described above (Fig. 1*C*).

It is important to consider how the macroH2A C-terminal linker and macro domain affect the shape and size of the nucleosomal arrays using the sedimentation coefficient distribution, relative to canonical H2A. Restriction digestion analysis of $macroH2A_{FL}$ and major-type H2A arrays showed 4–5% free DNA (supplemental Fig. 1*B*), consistent with a fully saturated array (17). Both types of arrays sediment with an s_{avg} of 28–29 S for fully saturated and 25–26 S for subsaturated arrays. We conclude that the macro domain and linker domain in $macroH2A_{FL}$ do not promote additional interactions under these conditions (*e.g.* through interactions of two macro domains). The combined mass of 207 base pairs of DNA and a histone octamer is 235 kDa. Substitution of two molecules of major-type H2A with macroH2A in each histone octamer increases the mass by 54 kDa. If there were no effect on the frictional coefficient (as $S \approx M/F$), one might expect a saturated array containing macroH2A to sediment more quickly (with a sedimentation coefficient greater than 29 S) compared with the major-type H2A-containing array. However, we do not observe a change in the sedimentation coefficients for major type H2A and $macroH2A_{FL}$ arrays. Therefore, data from AUC and restriction enzyme digestion assays suggest that the increased molecular weight of $macroH2A_{FL}$ arrays is compensated for by an increase in the frictional coefficient in low salt buffer.

The Linker Region of MacroH2A Induces Salt-dependent, Hyper-responsive Oligomerization of Nucleosomal Arrays—Short range nucleosome-nucleosome interactions are induced in 12-mer polynucleosomes at relatively low (<1.5 mM) $MgCl_2$ concentrations, leading to the formation of 30-nm fiber-like structures (23). These interactions result in an overall shortening of the array and closely mimic the transitions of native chromatin upon the addition of low concentrations of divalent (and higher concentrations of monovalent) salts (24). This structural transition has been successfully studied for various nucleosomal arrays using sedimentation velocity where moderately folded arrays sediment at ~40 S, and completely folded arrays sediment at ~55 S (16, 19, 20, 21, 32). The final condensation occurs at higher $MgCl_2$ levels, where multiple arrays condense cooperatively to produce particles sedimenting at >60 S defined as self-association or oligomerization (20, 32). To determine the effect of $macroH2A_{FL}$ and the two truncated forms of macroH2A on chromatin condensation, we incubated saturated arrays with 0.5 or 0.75 mM $MgCl_2$ and analyzed them by sedimentation velocity.

Arrays containing major-type H2A exhibit only a very limited degree of folding at both concentrations of $MgCl_2$ (0.5 and 0.75 mM), as indicated by the midpoint S increase from ~28 S to ~30 and 33 S, respectively (Fig. 2*A*), and as reported previously (25). The distribution as a whole shifts to the right, demonstrating that all arrays within the sample, independent of the saturation, are susceptible to moderate salt-induced folding. Arrays containing $macroH2A_{FL}$ display a very similar response to $MgCl_2$, achieving 31 and 34 S in the presence of increasing $MgCl_2$ (Fig. 2*B*). Arrays with macroH2A(1–122) (Fig. 2*C*) behave similarly to the arrays with $macroH2A_{FL}$ (Fig. 2*B*) and major-type H2A (Fig. 2*A*) except for a slightly higher tendency to form 40–55 S species in the presence of 0.75 mM $MgCl_2$ (Fig. 2*C*). In striking contrast, arrays containing macroH2A(1–161) behaved unlike any other type of nucleosomal array previously studied (Fig. 2*D*). The bottom 40% of the boundary shows folding behavior very similar to that of major-type H2A and $macroH2A_{FL}$ (compare supplemental Fig. 2*A* with Fig. 2, *A* and *B*). However, the upper ~50–60% of macroH2A(1–161) sedimented as much larger particles (>60–120 S) (Fig. 2*D*) when compared with the other samples under similar ionic conditions. The sedimentation curve shows a clear separation between the rapidly sedimenting, hyper-responsive population (>60 S) and a slower sedimenting population represented by the lower half of the curve (~35 S) (compare the *top half* and *bottom half* of Fig. 2*D*). The position of the transition point (between particles equal to and larger than 60 S) suggests that only arrays containing at least 11 nucleosomes (>26 S) are hyper-responsive to salt (Fig. 2, *D* and *E*).

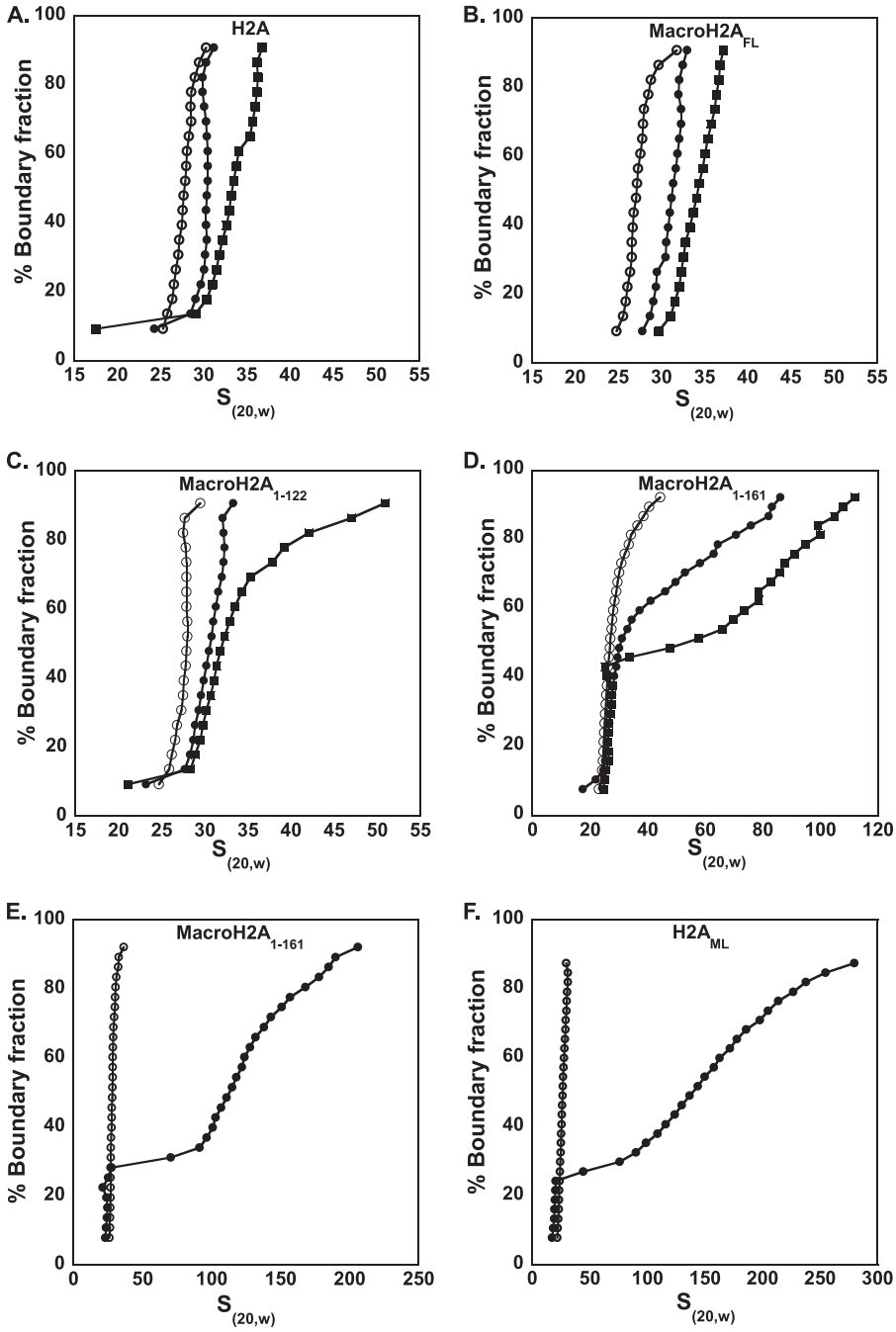

FIGURE 2. **The linker region of macroH2A facilitates oligomerization of nucleosomal arrays at very low $MgCl_2$ concentrations.** Sedimentation velocity experiments were performed for the different arrays in the absence or presence of 0.5, 0.75, or 1 mM $MgCl_2$. In all experiments, *open circles* represent arrays without $MgCl_2$. In *A–D*, *closed circles* represent arrays in 0.5 mM $MgCl_2$, and *closed squares* represent arrays in 0.75 mM $MgCl_2$. Experiments shown in *E* and *F* were done in the presence of 1 mM $MgCl_2$ (*closed circles*). *A*, arrays with H2A; *B*, arrays with macroH2A$_{FL}$; *C*, arrays with macroH2A(1–122); *D*, arrays with macroH2A(1–161); *E*, arrays with macroH2A(1–161) (1 mM $MgCl_2$); *F*, arrays with H2A$_{ML}$ (1 mM $MgCl_2$).

Our results suggest a unique role of the macroH2A linker region in promoting array oligomerization at low $MgCl_2$ concentrations. Therefore, we wanted to test whether the linker domain would function similarly in the context of major-type nucleosomal arrays. We compared the folding behavior of ~27 S arrays containing macroH2A(1–161) with those containing a version of major-type H2A with the macroH2A linker domain (amino acids 123–161) fused to the C terminus (H2A$_{ML}$; Fig. 2, *E* and *F*). The two arrays containing the macroH2A linker exhibit overlapping $G(s)$ distributions with a nearly identical fraction (~75%) of both arrays sedimenting as 60–200 S particles. This comparison demonstrates that the macroH2A linker domain alone is responsible for the hyper-sensitive salt-dependent condensation (for a more detailed representation of the *bottom half* of the curves, see supplemental Fig. 2, *B* and *C*).

To exclude the possibility that the behavior of macroH2A(1–161) was dependent on the unique properties of the 601 positioning sequence, we repeated all folding experiments with arrays reconstituted onto a weaker nucleosome-positioning sequence, the 5 S rDNA 208-12 template (26), with essentially

TABLE 2
Summary of folding studies done in the presence of 1 mM $MgCl_2$ for arrays assembled on two different DNA sequences, 601 207-12 and 5 S 208-12
Arrays were analyzed by sedimentation velocity AUC to determine s_{avg} in the absence or presence of 1 mM $MgCl_2$. ND, not done.

	0 mM $MgCl_2$		1 mM $MgCl_2$	
H2A construct	601 207-12	5 S 208-12	601 207-12	5 S 208-12
H2A	26 S	27.5 S	31 S	31 S
MacroH2A$_{FL}$	29 S	26.5 S	34 S	30 S
MacroH2A(1–161)	26 S	26.5 S	30–300 S[a]	20–300 S[a]
MacroH2A(1–122)	28 S	29 S	35 S	36.5 S
H2A$_{ML}$	26.5 S	ND	30–300 S[a]	ND

[a] For macroH2A(1–161) and H2A$_{ML}$ arrays, it is not possible to define a midpoint *S* value; therefore, the entire range is given.

the same results. Table 2 shows a comparison of the data obtained with the two DNA sequences. Together, our data suggest that in the presence of low concentrations of $MgCl_2$, the unstructured C-terminal macroH2A linker domain greatly facilitates and/or stabilizes the formation of higher order compacted chromatin structures. This behavior is only observed in the absence of the macro domain of macroH2A.

A Threshold Nucleosome Density Is Required in MacroH2A(1–161) Arrays to Undergo Oligomerization—To test the hypothesis that only arrays containing 11 nucleosomes or more are hyper-responsive to salt, we assembled arrays containing macroH2A(1–161) with varying degrees of undersaturation. This was accomplished by using subsaturating levels of tetramer (4–8 $(H3\text{-}H4)_2$ tetramers per 207-12 DNA) and varying amounts of dimer. Array saturation was confirmed by sedimentation velocity (Fig. 3, *A*, *C*, *E*, and *G*) and EcoRI digestion (supplemental Fig. 1, compare *B* and *C*). Note that no free 207-12 DNA (2484 bp) was present in the arrays despite the subsaturating levels of H3-H4 tetramer (Fig. 3 and supplemental Fig. 1*C*). Fig. 3 shows a range of arrays with s_{avg} values of 15, 17, 18, and 19 S (corresponding to a range of 4–8 nucleosomes/array) (31) (Fig. 3, *A*, *C*, *E*, and *G*, and Table 3). The 15 and 17 S arrays did not exhibit any 55–300 S particles (Fig. 3, *B* and *D*) when treated with 1 mM $MgCl_2$. Instead, an intermediate stage of folding with slightly higher *s* value is observed. 15 S arrays condense to an s_{avg} of ~19S (Fig. 3*B*). 17 S arrays condense to give an s_{avg} of ~21 S, but ~20% of these arrays folded to 25–30 S species (Fig. 3*D* see top of +$MgCl_2$ curve and Table 3). However, an increase in nucleosome density on the 207-12 DNA template in the 18 and 19 S arrays resulted in increasing oligomerization in the presence of $MgCl_2$ (Fig. 3, *F* and *H*). In Fig. 3*F*, ~20% of the array population self-associates to form the 40–150 S particles. This population is probably the ~20% of arrays that are at ~22 S in the absence of $MgCl_2$ (Fig. 3*E*). Similarly, ~40% of the 19 S arrays self-associate to form 40–160 S particles reflecting the 40% of species at ~20 S or more (Fig. 3, *G* and *H*). A detailed view of the lower half of the sedimentation velocity curves for data in Fig. 3, *F* and *H*, is shown in supplemental Fig. 2, *E* and *F*, respectively. Thus, using these extremely undersaturated arrays, we were able to ascertain that macroH2A(1–161) arrays were sensitive to $MgCl_2$ even at an extremely low nucleosome density of ~8.

The increased sensitivity to 1 mM $MgCl_2$ with increasing nucleosome density for macroH2A(1–161) arrays was confirmed by analyzing the above mentioned samples by SDS-PAGE. Arrays were incubated with 1 mM $MgCl_2$ for 5 min at room temperature and spun at 14,000 rpm (~20,000 × *g*) for 5 min. This sediments ≥300 S particles, leaving anything smaller in solution (28). The supernatant and pellets were analyzed on a 15% SDS-polyacrylamide gel. Control tetrasome arrays and 15 S macroH2A(1–161) arrays were completely soluble under these conditions (Fig. 3*I*, *lanes 2* and *4*), whereas an increasing percentage of the material precipitates in both 17 S arrays (Fig. 3*I*, *lanes 5* and *6*) and 19 S arrays (Fig. 3*I*, *lanes 7* and *8*). This material is probably represented by the faster sedimenting upper part of the sedimentation velocity curves *above* (Fig. 3, *F* and *H*).

Together, these results indicate that macroH2A(1–161) is capable of salt-dependent hyper-responsive oligomerization even at very low nucleosome occupancy (~5–6 nucleosomes/12-mer array; Table 3) and exhibits $MgCl_2$-induced compaction at an even lower occupancy (~4) (Fig. 3, *A–D*, and Table 3).

The Hyper-responsive Oligomerization of MacroH2A(1–161) Arrays Is Reversible—It has previously been shown using both native chromatin fibers (27) and model nucleosome arrays (28) that salt-dependent oligomerization is reversible. We questioned whether this was also true for macroH2A(1–161) arrays. To test this, ~25 S arrays containing macroH2A(1–161) were treated with 1 mM $MgCl_2$ as in Fig. 2*E*, resulting in oligomerization. The arrays were dialyzed overnight against buffer lacking $MgCl_2$. We then subjected the dialyzed arrays as well as the original untreated arrays and arrays freshly treated with 1 mM $MgCl_2$ to sedimentation velocity experiments. The untreated arrays and those treated with 1 mM $MgCl_2$ prior to dialysis sedimented nearly identically and exhibited no signs of folding or oligomerization (supplemental Fig. 2*D*). Thus, the salt-dependent oligomerization of macroH2A(1–161) arrays is readily reversed by removal of $MgCl_2$, arguing against the possibility that the observed extreme behavior of macroH2A(1–161) arrays is the result of non-native aggregation or precipitation.

The Linker Region of MacroH2A Promotes Fiber-Fiber Interactions in Nucleosomal Arrays—To understand the effect of various macroH2A domains on internucleosomal array interactions, we subjected all arrays to a self-association assay. This assay mimics the long range fiber-fiber interactions observed in cellular chromatin (24), by measuring the oligomerization state of arrays as a function of $MgCl_2$ concentration (23, 28). Nucleosomal arrays reconstituted with the different major-type and macroH2A constructs were subjected to increasing concentrations of $MgCl_2$, followed by a brief centrifugation as described above (~20,000 × *g*, 5 min) to determine the fraction of each array remaining in the supernatant (Fig. 4*A*). All arrays exhibited an initial dip in the oligomerization curve at very low $MgCl_2$ concentrations (<0.5 mM), most likely because slightly overassembled arrays (>12 nucleosomes/template; >30 S; see

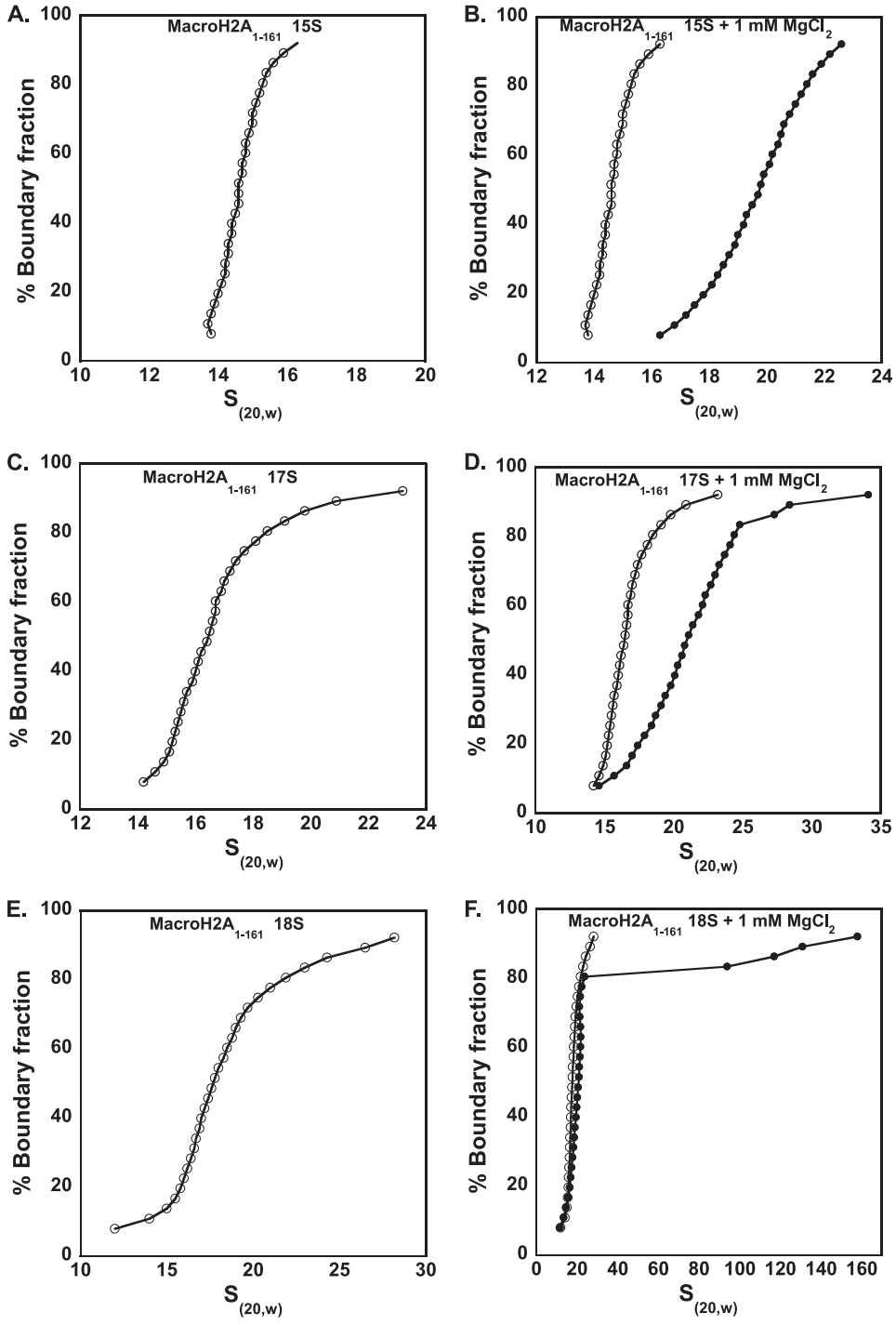

FIGURE 3. **Nucleosome occupancy affects the oligomerization properties of macroH2A(1–161) arrays.** Sedimentation velocity experiments were performed for macroH2A(1–161) arrays at various saturation levels of the dimer (giving rise to 4–8 nucleosomes; see Table 3) in the absence (*open circles*) and presence (*closed circles*) of 1 mM $MgCl_2$. *A*, 15 S arrays; *B*, 15 S arrays treated with 1 mM $MgCl_2$; *C*, 17 S arrays; *D*, 17 S arrays folding in the presence of 1 mM $MgCl_2$; *E*, 18 S arrays; *F*, 18 S arrays treated with 1 mM $MgCl_2$. *G*, 19 S arrays; *H*, 19 S arrays treated with 1 mM $MgCl_2$; *I*, SDS-PAGE analysis of control tetrasome arrays and 15 17, and 19 S macroH2A(1–161) arrays in the absence and presence of 1 mM $MgCl_2$. Soluble (*S*) and insoluble (*P*) fractions were analyzed on a 15% SDS-polyacrylamide gel. With increasing nucleosome density on macroH2A(1–161) arrays, more of the sample is seen in the pellet (*P*). *Lanes 9* and *10*, macroH2A(1–161)-H2B dimer and $(H3\text{-}H4)_2$ tetramer, respectively. The 19 S (*P**) lane had a split in the well, and hence the same sample appears as *two lanes*.

Fig. 1*C*) are particularly sensitive to $MgCl_2$. Arrays reconstituted with $macroH2A_{FL}$ or with macroH2A(1–122) behaved very similarly to arrays containing major-type H2A. The resulting Mg_{50} values (the concentration of $MgCl_2$ at which 50% of the array is soluble) were nearly identical (between 1.7 and 1.85 mM) (Fig. 4*C*). This indicates that the macro domain neither enhances nor inhibits long range fiber-fiber interactions. In contrast, nucleosomal arrays reconstituted with macroH2A(1–161) required much less $MgCl_2$ for oligomerization (Mg_{50} = 1.0) (Fig. 4*C*). Oligomerization assays were repeated with

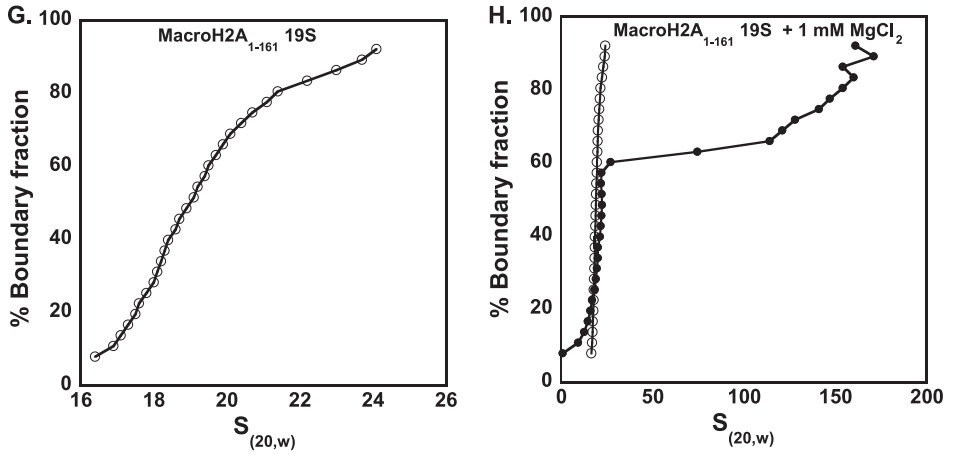

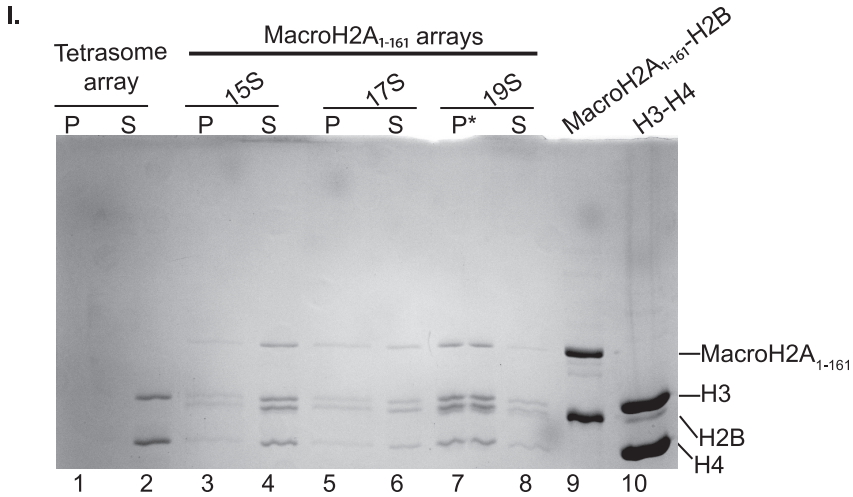

FIGURE 3—*continued*

TABLE 3

Summary of folding studies performed on undersaturated arrays containing macroH2A(1–161)-H2B dimers show a steady progression in the formation of 30-150 S particles with increasing nucleosome density indicative of oligomerization

Extremely subsaturated arrays were assembled by limiting the number of $(H3\text{-}H4)_2$ tetramers (*R* value of 0.7), and by varying the amount of macroH2A(1–161)-H2B dimer (*R* values between 0.8 and 1.4). The arrays were subjected to sedimentation velocity AUC in the absence and presence of 1 mM $MgCl_2$. The percentage of folded and oligomerized species is given in parentheses where applicable.

R value[a] of macroH2A(1–161)-H2B	s_{avg} 0 mM $MgCl_2$	Number of particles[b] (based on s_{avg})	s_{avg}[c] 1 mM $MgCl_2$
0.8	15 S	~4	19 S
1.0	17 S	~6	21 S (80%)[d] 22–35 S (20%)[e]
1.2	18 S	~6–7	22S (80%)[d] 30–150 S (20%)[e]
1.4	19 S	~7–8	22S (60%)[d] 30–160 S (40%)[e]

[a] *R* value is the ratio of macroH2A(1–161)-H2B dimer titrated per repeat of 207-bp nucleosomal DNA during array reconstitution while the H3-H4 *R* value was held constant at 0.7.
[b] As described in Ref. 31.
[c] See Fig. 3 and Supplemental Fig. 2, *E* and *F*.
[d] Percentage folded population.
[e] Percentage oligomerized population.

smaller increments of $MgCl_2$ for macroH2A(1–161) arrays, to determine the midpoint of oligomerization with better resolution (Fig. 4*B*). Arrays reconstituted with $H2A_{ML}$ behaved nearly identically to macroH2A(1–161) (Mg_{50} = 1.0), demonstrating that the linker region is sufficient for the increased propensity to form fiber-fiber interactions (Fig. 4, *A* and *C*).

The Salt-dependent Oligomerization of the Arrays Is Not Due to Non-stoichiometric Histone Composition—We next wanted to test whether the hyperresponsive condensation behavior of macroH2A(1–161) arrays in the presence of $MgCl_2$ was due to non-canonical nucleosomes formed as a result of unusual histone stoichiometry. In particular, we wanted to test the possibility that the upper, most salt-sensitive fraction of the boundary (*e.g.* Fig. 2, *D–F*) might contain arrays with an aberrant stoichiometry of histones, indicating improperly assembled nucleosomes; such arrays might respond differently to the addition of salt. To test this possibility, we incubated ~25 S arrays with 1 mM $MgCl_2$, where a significant portion of the arrays

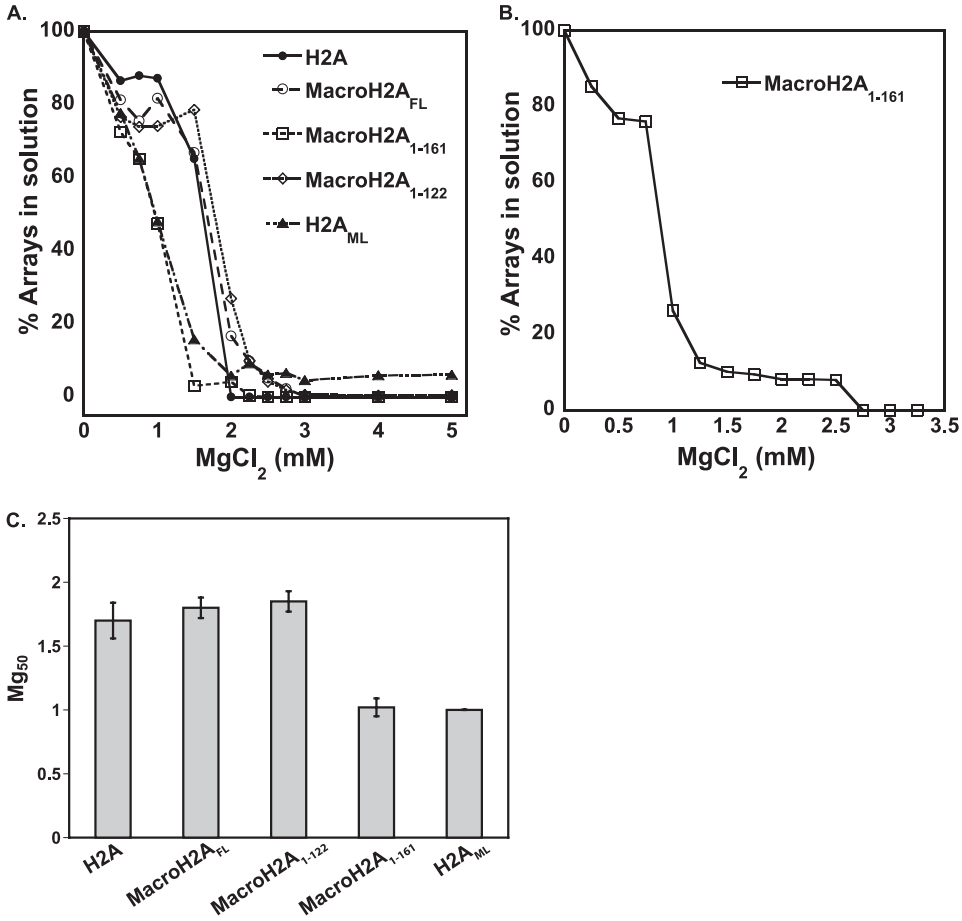

FIGURE 4. **The linker region of macroH2A promotes fiber-fiber interactions.** *A*, self-association curves obtained from differential centrifugation assays for all arrays are shown. Each array was incubated with increasing amounts of $MgCl_2$ and centrifuged (at ~20,000 × *g* for 5 min) to remove the insoluble fraction. The percentage of soluble array was calculated and plotted. The initial dip in the curve represents the oversaturated population (>30 S) in the arrays. *B*, self-association assay performed at smaller increments of $MgCl_2$ for macroH2A(1–161) confirmed the Mg_{50} value. *C*, Mg_{50} values (defined as the $MgCl_2$ concentration required to oligomerize 50% of arrays out of solution) from 2–5 iterations of self-association are plotted as *bar graph* for all arrays except for $H2A_{ML}$, where it was performed only once. *Error bars*, S.D. values calculated from multiple experiments.

containing macroH2A(1–161) or $H2A_{ML}$ form large, insoluble oligomers (Fig. 2, *E* and *F*), whereas arrays with H2A, $macroH2A_{FL}$, and macroH2A(1–122) are largely soluble. The soluble (*S*) and insoluble (*P*) fractions were separated by differential centrifugation and analyzed by SDS-PAGE (Fig. 5, *A–C*). $MacroH2A_{FL}$ (Fig. 5*A*, *lanes 2* and *3*), macroH2A(1–122) (Fig. 5*A*, *lanes 6* and *7*), and major-type H2A containing arrays (Fig. 5*A*, *lanes 8* and *9*) remained mostly soluble (with stoichiometric histone content) at 1 mM $MgCl_2$ (compare insoluble (*P*) and soluble (*S*) *lanes* for each array). Due to its higher sensitivity to salt, most of the macroH2A(1–161) array was found in the pellet (*P*) under these conditions (Fig. 5*A*, *lanes 4* and *5*). $H2A_{ML}$-containing arrays behaved similarly to macroH2A(1–161) (Fig. 5*B*, *lanes 11* and *12*). Neither of these arrays deviated in the stoichiometry of the histones present in the folded *versus* oligomerized arrays under conditions that favor folding. These same arrays were also treated with 5 mM $MgCl_2$, where 100% of the arrays oligomerize (Fig. 5, *B* (*lane 13*) and *C* (*lanes 17*, *20*, *22*, and *24*)). In all cases (along with the histone content of untreated arrays shown in Fig. 1*B*), the distribution and stoichiometry of the histones did not vary among the arrays. These experiments support the conclusion that the unusual oligomerization behavior of macroH2A(1–161)-containing arrays is not caused by a non-stoichiometric or an otherwise atypical distribution of histones.

Atomic Force Microscopy reveals "Macro" Particles in Response to $MgCl_2$—AFM was used to obtain independent evidence for the condensation behavior of the various nucleosomal arrays studied by AUC and differential centrifugation. Arrays used for AFM imaging were closely matched in saturation (supplemental Fig. 3*A*) and were subjected to imaging in air after preincubation with 0.5 mM $MgCl_2$. Supplemental Fig. 3*C* shows a representative individual major-type array containing 12 nucleosomes with height profiles between 1.5 and 2.5 nm (supplemental Fig. 3*D*), with the linker DNA clearly visible. The height profiles are consistent with those previously reported by others (29). The majority of the ~27 S arrays used for imaging contained 9–10 nucleosomes (supplemental Fig. 3*B*), in excellent agreement with the AUC results (16).

Representative images of 2 × 2 μm scans for each array in the absence or presence of $MgCl_2$ are shown in Fig. 6. The wider scan fields allowed us to scan for the free, folded, and oligomerized populations of arrays that were observed in the sedimentation velocity experiments. Multiple images were analyzed for each array in the presence or absence of 0.5 mM $MgCl_2$, and the

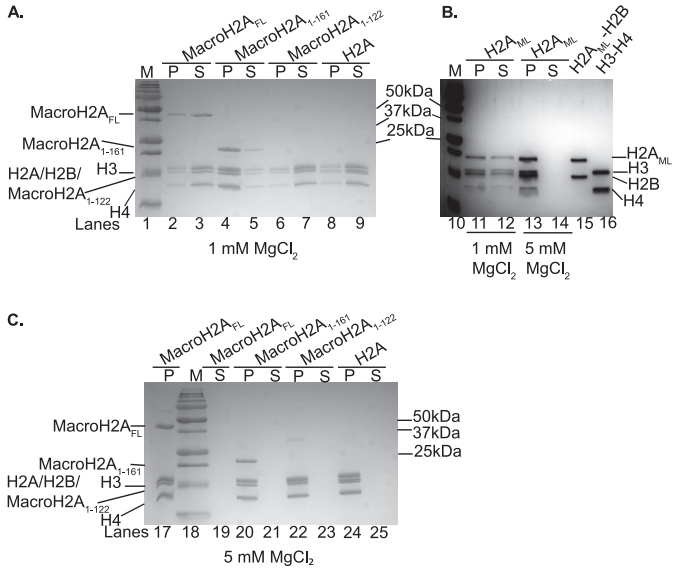

FIGURE 5. **The salt-dependent oligomerization of the arrays is not a result of uneven histone composition.** *A*, arrays were incubated with 1 mM $MgCl_2$ and centrifuged to separate the soluble (*S*) and insoluble (*P*) fractions, which were then analyzed on a 15% SDS-polyacrylamide gel. *Lanes 1*, *10*, and *18*, protein size markers (*M*); *lanes 15* and *16*, $H2A_{ML}$-H2B dimer and $(H3\text{-}H4)_2$ tetramer, respectively. Nearly all arrays remain mostly soluble (*S*) in the presence of 1 mM $MgCl_2$, whereas macroH2A(1–161) is mostly in the pellet (*P*) (*lane 4*). Note that all four histones are present in the soluble and insoluble fractions of all arrays. *B*, $H2A_{ML}$ arrays treated with 1 and 5 mM $MgCl_2$ behave similar to arrays assembled with macroH2A(1–161). *C*, arrays were treated with 5 mM $MgCl_2$, rendering all material insoluble.

height distribution histograms of several hundred nucleosomes are shown in Fig. 6 (*right*). Arrays assembled only with $(H3\text{-}H4)_2$ tetramers are shown in supplemental Fig. 4 and are clearly distinguishable in their height profile from the nucleosome arrays shown in Fig. 6.

Arrays with major-type H2A look very similar in the absence and presence of 0.5 mM $MgCl_2$ (Fig. 6*A*, *left* and *middle*) as predicted from their sedimentation behavior (Fig. 2*A*). Height profiles for both samples cluster around 1–1.5 nm (Fig. 6*A*; *histogram* in the *right panel*) in excellent agreement with the published height profiles for nucleosomes (28). Likewise, arrays with $macroH2A_{FL}$ display well separated nucleosomes in the absence and presence of 0.5 mM $MgCl_2$ (Fig. 6*B*) with a similar height profile distribution (compare histograms in Fig. 6, *A* and *B*). It is important to note that no increase in height profiles is observed for $macroH2A_{FL}$ arrays despite an increase in molecular weight of H2A because the macro domain is likely to be randomly oriented because of the flexible nature of the linker region. Nucleosomal arrays reconstituted with macroH2A(1–122) are also characterized by well separated nucleosomes (Fig. 6*C*, *left*) in the absence of $MgCl_2$. Upon treatment with 0.5 mM $MgCl_2$, these arrays exhibit minor compaction (Fig. 6*C*, *middle*), but larger particles were absent. The height distribution in the absence of $MgCl_2$ is very similar to that observed for major-type H2A arrays but is shifted toward particles that are between 1.5 and 2 nm in height in the presence of 0.5 mM $MgCl_2$ for macroH2A(1–122) arrays (Fig. 6*C*, *histogram*). This is in close agreement with its higher propensity to fold without oligomerization as observed in the sedimentation velocity experiments (Fig. 2*C*). As anticipated from the AUC experiments, arrays with macroH2A(1–161) or $H2A_{ML}$ exhibit a dramatically different behavior. The majority of both arrays exhibit clearly discernible chains of nucleosomes with the canonical height profiles in the absence of $MgCl_2$ (Fig. 6, *D* and *E*). However, in the presence of 0.5 mM $MgCl_2$, two distinct populations of macroH2A(1–161) and $H2A_{ML}$ arrays are observed (Fig. 6, *D* and *E*, *middle panels*). There are individual, mostly undersaturated arrays (~25–27 S) in which the height profile for the nucleosome ranges from 1.5 to 2 nm. The second population consists of a much larger species with height profiles between 3 and 80 nm representing the rapidly sedimenting population of >55 S seen in AUC experiments (Fig. 6, *D* and *E*, for AFM; Fig. 2, *D–F*, for AUC). Thus, the data obtained in AFM studies are complementary to the results from the AUC experiments.

DISCUSSION

The incorporation of variant histones has the potential to alter chromatin structure and regulate access to nucleosomal DNA. In the present study, we have analyzed various constructs of macroH2A and major-type H2A to dissect the contribution of the two domains that are unique to macroH2A toward chromatin structure regulation. Using AUC and AFM with *in vitro* reconstituted nucleosomal arrays, we have shown that arrays reconstituted with full-length macroH2A exhibit similar folding and self-association behavior as their major-type counterparts. The addition of a 32-kDa domain affects neither folding nor self-association of the arrays. In contrast, removal of the macro domain alone, leaving the linker region intact, results in an extreme and highly $MgCl_2$-sensitive self-association behavior. To the best of our knowledge, this is the first characterization of the condensation properties of nucleosomal arrays containing this enigmatic histone variant.

Heterochromatin is defined as the densely packed and transcriptionally inactive regions of chromatin in the interphase nucleus. MacroH2A localizes to heterochromatin on the inactive X chromosome as well as to senescence-related heterochromatin, but how it contributes to heterochromatin compaction is unknown. There is evidence that macroH2A nucleosomes are more stable than their major-type counterpart *in vitro*. MacroH2A1.2-containing nucleosomes were stable in up to 1.5 M NaCl, whereas the major-type nucleosomes started to dissociate above 0.9 M NaCl (30). If and how this increased stability translates to the condensation of the chromatin fiber is unknown. For example, nucleosomes containing macroH2A are more resistant toward chaperone-mediated histone exchange (9). Previous research from our laboratory has shown that macroH2A preferentially forms hybrid mononucleosomes in which one canonical H2A and one macroH2A dimer are combined. However, attempts to reconstitute hybrid nucleosome arrays resulted in heterogeneous array populations, and the approaches used to isolate heterotypic mononucleosomes cannot be applied to arrays. We are currently developing alternative approaches to prepare homogenous "designer arrays."

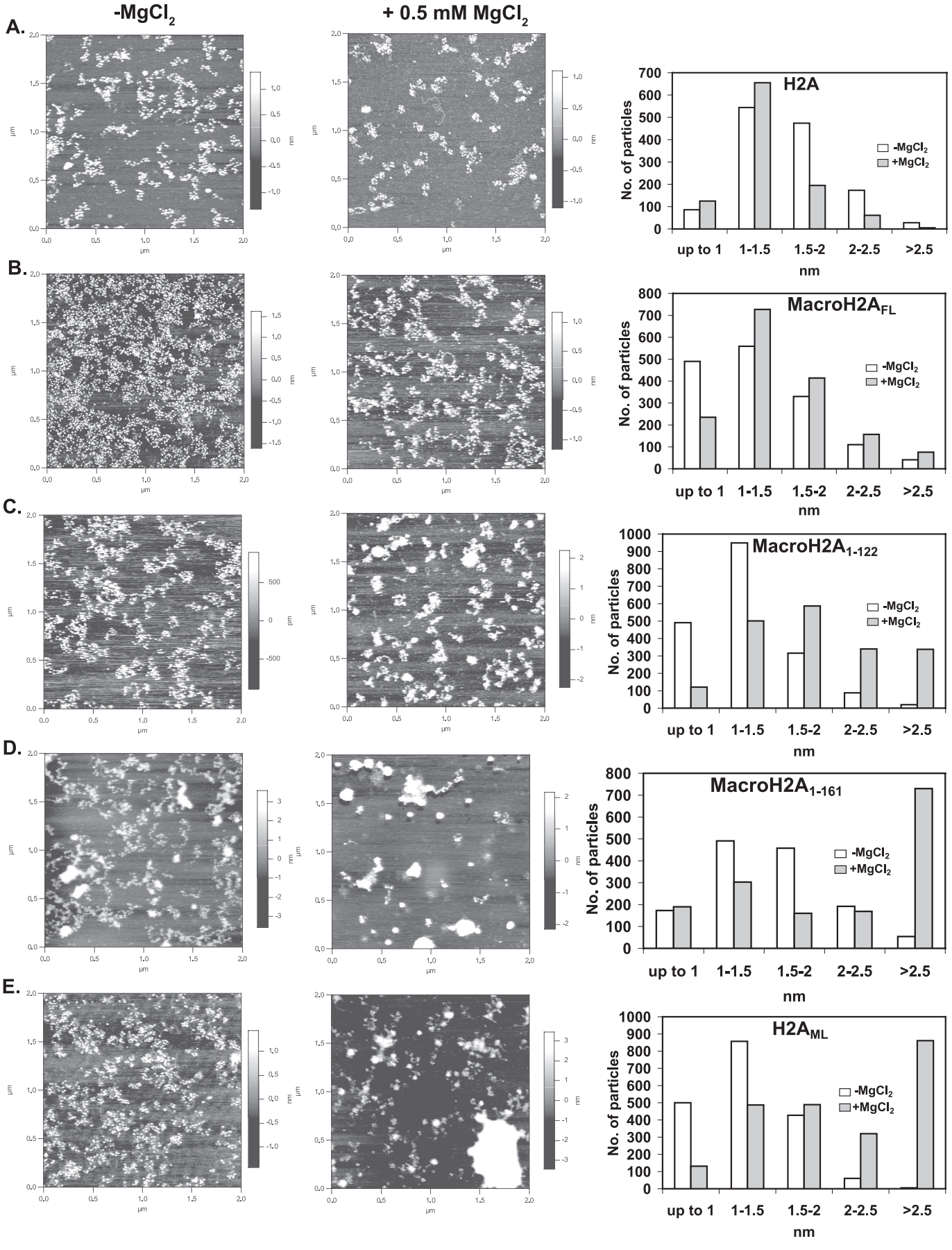
-MgCl2
+ 0.5 mM MgCl2
A.
B.
C.
D.
E.
H2A
MacroH2AFL
MacroH2A1-122
MacroH2A1-161
H2AML
-MgCl2
+MgCl2
No. of particles
up to 1
1-1.5
1.5-2
2-2.5
>2.5
nm

The assays used here allowed us to distinguish partially to fully folded nucleosome arrays that sediment at ~40–55 S from self-associated (oligomerized) particles that sediment at >60 S (20, 32). Surprisingly, no significant differences between arrays reconstituted with full-length macroH2A and arrays with major-type H2A were observed in highly sensitive assays that probe array folding and fiber-fiber self-association. These assays are widely accepted as *in vitro* models for 30-nm fiber formation and higher order chromatin architecture. This result is consistent with our findings that the disconnected macro domain does not associate measurably with nucleosomes or chromatin arrays *in vitro*[3] and indicates that the macro domain of H2A does not contribute to nucleosome-nucleosome interactions. Additionally, purified macro domain added to macroH2A(1–161) arrays in *trans* did not reverse the sensitivity of the arrays to $MgCl_2$ (data not shown). Arrays reconstituted with the histone region of macroH2A behave no differently from major-type nucleosome arrays in folding and self-association assays. In contrast, arrays reconstituted with versions of macroH2A or major-type H2A that contain the linker region of macroH2A (but not the macro domain) exhibit highly cooperative $MgCl_2$-dependent self-association at much lower concentrations of $MgCl_2$, to a point where array folding is hardly observed. At 0.5 mM $MgCl_2$, a concentration where other arrays normally display intranucleosomal array interactions, macroH2A(1–161) arrays exhibit a unique sedimentation profile that indicates large scale oligomerization, resulting in large 60–120 S particles. Surprisingly, even extremely subsaturated macroH2A(1–161) arrays exhibit a certain degree of oligomerization. There are two likely criteria that determine whether the macroH2A(1–161)-containing arrays will self-associate: first, the presence of a sufficient number of intact nucleosomes containing macroH2A(1–161) and, second, the proximity of these nucleosomes on a given array. For example, the arrays shown in Fig. 3*C* contain ~10% of the 20–22 S species yet do not undergo oligomerization. This suggests that the $MgCl_2$-induced oligomerization of the macroH2A(1–161) arrays is observed only at a nucleosome density of ~8–9 nucleosomes/array. Similar results were reported for arrays reconstituted with native chicken histones on 208-12 mer DNA, where hardly any folding was observed for arrays containing less than 9 nucleosomes/array (31), indicating that canonical H2A requires a threshold nucleosome occupancy in order to stabilize folded chromatin. We note that macroH2A(1–161)-containing arrays undergo $MgCl_2$-induced compaction at even lower occupancies (~4 nucleosomes; Table 3), as indicated by an increase in s_{avg} from 15 S to 19 S and from 17 S to 21–35 S for these extremely undersaturated arrays (Fig. 3, *C–F*). However, the hyper-responsive oligomerization of macroH2A(1–161) arrays is observed only at a nucleosome density of ~8–9 (Table 3). Thus, it appears that minimal nucleosome occupancy of 8–9 per 12-mer array is required for the hyper-responsive behavior in the presence of $MgCl_2$ observed for macroH2A(1–161) nucleosomal arrays.

We previously observed a similar, although less extreme responsiveness to $MgCl_2$ with arrays reconstituted with $H4K_c20Me_3$ (32). This modification is found predominantly in heterochromatin (33). Similarly, when unmodified, major-type arrays were incubated with 0.25–0.45 mM $MgCl_2$ in the presence of stoichiometric amounts of linker histone H1, 55 S particles were formed (13). In an independent experiment, we found that major-type arrays with stoichiometric amounts of H1 form 50–120 S particles in 1.1 mM $MgCl_2$ (data not shown). Because the amino acid composition of the macroH2A linker region resembles that of the C-terminal domain of linker histone H1 (Table 1 and supplemental material), we speculate that the macroH2A linker region might serve as an intrinsic linker histone-like component in macroH2A that might be activated upon proteolytic removal of the macro domain (see below). Intriguingly, a recent study has shown that macroH2A-containing chromatin fractions isolated from nuclei are devoid of H1 (30), suggesting that these two compositionally similar proteins do not coexist in chromatin.

AFM has become a powerful tool for studying chromatin architecture and dynamics (34–38). For example, Montel *et al.* showed that the replacement of H2A with H2A Bbd, another H2A variant, results in more "open" arrays (37). AFM has also been applied to study nucleosome dynamics using time lapse imaging (34). In our studies, we used AFM to test assembly and to visualize the folding and oligomerization properties of *in vitro* assembled arrays. The image shown in supplemental Fig. 3*A* clearly validates our approach. Importantly, the saturation levels inferred from AUC were corroborated by counting the number of nucleosomes in well separated arrays for each construct (*e.g.* supplemental Fig. 3*C*). The large 60–120 S particles observed for macroH2A(1–161) arrays were also visualized by AFM, with height profiles up to 80 nm. These particles are not tip artifacts as observed by Caño *et al.* (39) because unoligomerized and oligomerized arrays can be seen in the same image.

We have identified a novel property of the linker region of macroH2A. Our results suggest the possibility that the macro domain inhibits the chromatin condensing function of the linker region. This activity could potentially be regulated by a protein that binds to the macro domain or by a post-translational modification of the macro domain or the linker region. It is tempting to speculate that *in vivo* chromatin structure might be regulated by the proteolytic removal of the macro domain

[3] S. Chakravarthy and K. Luger, unpublished observations.

FIGURE 6. **AFM analysis of array condensation.** AFM images were collected as 2 × 2-μm scans in the absence (*left panels*) and in the presence of 0.5 mM $MgCl_2$ (*middle panels*). Height profile distributions are shown as *bar charts* in the *right panel*. Height profile measurements were plotted in MS Excel as number of particles (for folded/oligomerized samples, individual nucleosomes cannot be distinguished) in each height profile category. *A*, H2A arrays; *B*, macroH2A$_{FL}$ arrays; *C*, macroH2A(1–122) arrays; *D*, macroH2A(1–161) arrays; *E*, H2A$_{ML}$ arrays. Note that in the absence of $MgCl_2$, the height profile of all arrays is clustered around 1.5–2 nm. For H2A arrays, there is not much increase in populations with >2.5-nm height. For all of the others, there is an increase in the taller particles (>2.5 nm); however, the increase for macroH2A(1–161) and H2A$_{ML}$ is most dramatic.

from macroH2A-containing nucleosomes, consistent with the role of macroH2A in maintaining a highly compacted heterochromatic state. Proteolytic processing of histone H2A (40) and H3 (41), with potential roles in regulating chromatin structure, has been described. Our results indicate that a rather small subpopulation of proteolyzed macroH2A$_{FL}$ has the potential to dramatically compact chromatin. Thus, attempts to identify a proteolytic product of macroH2A(1–161) rely on extremely high sensitivity of detection. Efforts to identify proteolyzed macroH2A and the corresponding protease are currently ongoing.

Acknowledgments—We thank the protein expression and purification facility in biochemistry (Colorado State University) for providing histone aliquots and Pari Fields for 601 207-12 DNA. Kitty Brown's help with AFM imaging is greatly appreciated. We thank Heather Szerlong, Aaron Hieb, and Kitty Brown for critical reading of the manuscript.

REFERENCES

1. Kamakaka, R. T., and Biggins, S. (2005) *Genes Dev.* **19,** 295–310
2. Chakravarthy, S., Bao, Y., Roberts, V. A., Tremethick, D., and Luger, K. (2004) *Cold Spring Harb. Symp. Quant. Biol.* **69,** 227–234
3. Chakravarthy, S., Gundimella, S. K., Caron, C., Perche, P. Y., Pehrson, J. R., Khochbin, S., and Luger, K. (2005) *Mol. Cell. Biol.* **25,** 7616–7624
4. Gamble, M. J., Frizzell, K. M., Yang, C., Krishnakumar, R., and Kraus, W. L. (2010) *Genes Dev.* **24,** 21–32
5. Changolkar, L. N., and Pehrson, J. R. (2006) *Mol. Cell. Biol.* **26,** 4410–4420
6. Gamble, M. J., and Kraus, W. L. (2010) *Cell Cycle* **9,** 2568–2574
7. Kapoor, A., Goldberg, M. S., Cumberland, L. K., Ratnakumar, K., Segura, M. F., Emanuel, P. O., Menendez, S., Vardabasso, C., Leroy, G., Vidal, C. I., Polsky, D., Osman, I., Garcia, B. A., Hernando, E., and Bernstein, E. (2010) *Nature* **468,** 1105–1109
8. Nusinow, D. A., Sharp, J. A., Morris, A., Salas, S., Plath, K., and Panning, B. (2007) *J. Mol. Biol.* **371,** 11–18
9. Chakravarthy, S., and Luger, K. (2006) *J. Biol. Chem.* **281,** 25522–25531
10. Karras, G. I., Kustatscher, G., Buhecha, H. R., Allen, M. D., Pugieux, C., Sait, F., Bycroft, M., and Ladurner, A. G. (2005) *EMBO J.* **24,** 1911–1920
11. Ladurner, A. G. (2003) *Mol. Cell* **12,** 1–3
12. Hansen, J. C., Lu, X., Ross, E. D., and Woody, R. W. (2006) *J. Biol. Chem.* **281,** 1853–1856
13. Lu, X., Hamkalo, B., Parseghian, M. H., and Hansen, J. C. (2009) *Biochemistry* **48,** 164–172
14. Dyer, P. N., Edayathumangalam, R. S., White, C. L., Bao, Y., Chakravarthy, S., Muthurajan, U. M., and Luger, K. (2004) *Methods Enzymol.* **375,** 23–44
15. Lowary, P. T., and Widom, J. (1998) *J. Mol. Biol.* **276,** 19–42
16. Tse, C., Fletcher, T. M., and Hansen, J. C. (1998) *Proc. Natl. Acad. Sci. U.S.A.* **95,** 12169–12173
17. Carruthers, L. M., Tse, C., Walker, K. P., 3rd, and Hansen, J. C. (1999) *Methods Enzymol.* **304,** 19–35
18. Demeler, B., and van Holde, K. E. (2004) *Anal. Biochem.* **335,** 279–288
19. Hansen, J. C., Lebowitz, J., and Demeler, B. (1994) *Biochemistry* **33,** 13155–13163
20. Schwarz, P. M., and Hansen, J. C. (1994) *J. Biol. Chem.* **269,** 16284–16289
21. Carruthers, L. M., Bednar, J., Woodcock, C. L., and Hansen, J. C. (1998) *Biochemistry* **37,** 14776–14787
22. Tse, C., and Hansen, J. C. (1997) *Biochemistry* **36,** 11381–11388
23. Hansen, J. C. (2002) *Annu. Rev. Biophys. Biomol. Struct.* **31,** 361–392
24. Lu, X., Klonoski, J. M., Resch, M. G., and Hansen, J. C. (2006) *Biochem. Cell Biol.* **84,** 411–417
25. Fan, J. Y., Gordon, F., Luger, K., Hansen, J. C., and Tremethick, D. J. (2002) *Nat. Struct. Biol.* **19,** 172–176
26. Simpson, R. T., Thoma, F., and Brubaker, J. M. (1985) *Cell* **42,** 799–808
27. Olins, D. E., and Olins, A. L. (1972) *J. Cell Biol.* **53,** 715–736
28. Schwarz, P. M., Felthauser, A., Fletcher, T. M., and Hansen, J. C. (1996) *Biochemistry* **35,** 4009–4015
29. Qian, R. L., Liu, Z. X., Zhou, M. Y., Xie, H. Y., Jiang, C., Yan, Z. J., Li, M. Q., Zhang, Y., and Hu, J. (1997) *Cell Res.* **7,** 143–150
30. Abbott, D. W., Laszczak, M., Lewis, J. D., Su, H., Moore, S. C., Hills, M., Dimitrov, S., and Ausió, J. (2004) *Biochemistry* **43,** 1352–1359
31. Hansen, J. C., and Lohr, D. (1993) *J. Biol. Chem.* **268,** 5840–5848
32. Lu, X., Simon, M. D., Chodaparambil, J. V., Hansen, J. C., Shokat, K. M., and Luger, K. (2008) *Nat. Struct. Mol. Biol.* **15,** 1122–1124
33. Barski, A., Cuddapah, S., Cui, K., Roh, T. Y., Schones, D. E., Wang, Z., Wei, G., Chepelev, I., and Zhao, K. (2007) *Cell* **129,** 823–837
34. Shlyakhtenko, L. S., Lushnikov, A. Y., and Lyubchenko, Y. L. (2009) *Biochemistry* **48,** 7842–7848
35. Lohr, D., Wang, H., Bash, R., and Lindsay, S. M. (2009) *Methods Mol. Biol.* **464,** 123–138
36. Baker, A. M., Fu, Q., Hayward, W., Lindsay, S. M., and Fletcher, T. M. (2009) *Nucleic Acids Res.* **37,** 5019–5031
37. Montel, F., Menoni, H., Castelnovo, M., Bednar, J., Dimitrov, S., Angelov, D., and Faivre-Moskalenko, C. (2009) *Biophys. J.* **97,** 544–553
38. Filenko, N. A., Kolar, C., West, J. T., Smith, S. A., Hassan, Y. I., Borgstahl, G. E., Zempleni, J., and Lyubchenko, Y. L. (2011) *PLoS One* **6,** e16299
39. Caño, S., Caravaca, J. M., Martín, M., and Daban, J. R. (2006) *Eur. Biophys. J.* **35,** 495–501
40. Eickbush, T. H., Watson, D. K., and Moudrianakis, E. N. (1976) *Cell* **9,** 785–792
41. Duncan, E. M., Muratore-Schroeder, T. L., Cook, R. G., Garcia, B. A., Shabanowitz, J., Hunt, D. F., and Allis, C. D. (2008) *Cell* **135,** 284–294